Structural Roles of Subunit Cysteines in the Folding and Assembly of the DNA Packaging Machine (Portal) of Bacteriophage P22†

Arantxa Rodríguez-Casado and George J. Thomas, Jr.*

Division of Cell Biology and Biophysics, School of Biological Sciences, University of Missouri−Kansas City, Kansas City, Missouri 64110-2499

Received November 26, 2002; Revised Manuscript Received January 23, 2003

ABSTRACT: The DNA packaging machine (portal assembly) of bacteriophage P22 is constructed from 12 copies of a multidomain 725-residue subunit comprising a complex α/β fold. The portal subunit contains four cysteines (Cys 153, Cys 173, Cys 283, and Cys 516), which produce distinctive Raman markers in the spectral interval 2500−2600 cm^{-1} originating from S−H bond-stretching vibrations diagnostic of S−H···X hydrogen-bonding interactions. The Raman spectrum is unique in the capability to characterize cysteine sulfhydryl interactions in proteins and shows that portal cysteine environments are significantly altered by assembly (Rodriguez-Casado et al. (2001) *Biochemistry 40*, 13583−13591). We have employed site-directed mutagenesis, size-exclusion chromatography, and Raman difference spectroscopy to characterize the roles of portal cysteines in subunit folding and dodecamer assembly. The stability of the portal monomer is severely reduced by a Cys → Ser point mutation introduced at either residue 173 or 516. In the case of C516S, the destabilized monomer still forms portal rings, as visualized by negative-stain electron microscopy, whereas portal ring formation cannot be detected for C173S, which forms aberrant aggregates. The C283S mutant is a hyperstable monomer that is defective in portal ring formation. Interestingly, Cys 283 is suggested by secondary structure homology with the ϕ29 portal to be within a domain involved in DNA translocation. Conversely, the phenotype of the C153S mutant is close to that of the wild-type protein, implying that the sulfhydryl moiety of Cys 153 is not essential to formation of the native subunit fold and productive assembly dynamics. The present results demonstrate that cysteines of the P22 portal protein span a wide range of sulfhydryl hydrogen-bonding strengths in the wild-type assembly, that three of the four sulfhydryls play key roles in portal protein stability and assembly kinetics, and that substitution of a mutant seryl interaction (O−H···X) for a wild-type cysteinyl interaction (S−H···X) can either stabilize or destabilize the native fold depending upon sequence context.

The *Salmonella* bacteriophage P22 has been extensively employed as a model for icosahedral double-stranded (ds)[1] DNA virus assembly (Figure 1) (*1*, *2*). Much attention has been given to investigating the pathways of subunit folding and recognition in the construction of P22 sub-viral components, including the procapsid (*3*−*6*), capsid (*7*−*9*), tailspike (*10*−*12*), and portal sub-assemblies (*6*, *13*, *14*). The P22 portal, which is formed as a ring from 12 copies of a 725-residue (84 kDa) subunit, is incorporated into the procapsid shell at a unique 5-fold vertex. The portal provides the entry channel for packaging the viral genome during phage morphogenesis and the exit channel for releasing the dsDNA during host infection. The portal not only functions as a DNA-translocating machine in conjunction with nonstructural viral factors (terminase/ATP) but also interacts with the minor proteins that seal the portal after DNA packaging and reopen it for genome ejection. The portal additionally serves as a platform for mediating recognition of other viral structural proteins, including the coat protein in both its precursor (procapsid) and mature (capsid) forms and the trimeric tailspike protein that constitutes the host adhesin. These diverse roles suggest a highly versatile protein that comprises multiple recognition domains and has the capability to switch between different conformational states in a path-dependent manner.

Portal assemblies of several dsDNA bacteriophages have been investigated by structural, biochemical, and genetic methods (reviewed in refs *15* and *16*). Recently, three-dimensional reconstructions based upon the data of X-ray diffraction and electron cryomicroscopy have been reported by two independent groups for the dodecameric portal machine (connector) of bacteriophage ϕ29 (*17*−*20*). No equivalent structural detail is available for either the portal assembly of P22 or genome packaging channels of other viruses. The ϕ29 and P22 portal subunits differ dramatically in size (36 vs 84 kDa) and exhibit no significant sequence homology. However, residues 240−340 of the P22 subunit appear to contain considerable secondary structure homology with residues 125−235 of the ϕ29 subunit: Alternating

† This is paper LXXVII in the series Structural Studies of Viruses by Raman Spectroscopy. Supported by NIH Grant GM50776.

* To whom correspondence should be addressed. E-mail: thomasgj@umkc.edu. Telephone: (816) 235-5247. Fax: (816) 235-1503.

[1] Abbreviations: ds, double-stranded; EM, electron microscopy; HPSEC, high-performance size-exclusion chromatography; IPTG, isopropyl-β-D-thiogalactoside; MALDI−TOF, matrix-assisted laser desorption ionization−time-of-flight; MS, mass spectrometry; PAGE, polyacrylamide gel electrophoresis; PCR, polymerase chain reaction; SDS, sodium dodecyl sulfate; WT, wild type.

10.1021/bi020678m CCC: $25.00
Published on Web 03/07/2003

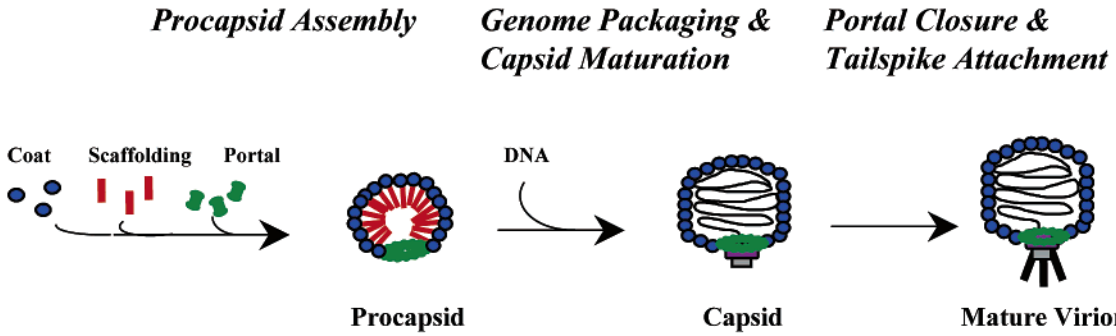

FIGURE 1: Assembly of *Salmonella* phage P22 (*1*, *30*). Construction of the procapsid (left) requires 420 copies of the coat subunit (blue), ~300 copies of the scaffolding subunit (red), and 12 copies of the portal subunit (green), together with a few copies of minor proteins (not shown). Subsequent genome packaging and maturation of the capsid (middle) is accompanied by scaffold ejection in an ATP-driven process directed by virally encoded factors. Portal closure by addition of minor proteins and tailspike attachment yields the mature virion (right).

α-helical and β-stranded modules in the φ29 X-ray structure map closely with the predicted secondary structure of the P22 portal protein and are consonant with the Raman amide band signatures (*13*). Interestingly, this apparent structural homology involves the inner annular surface of the φ29 portal channel and suggests that residues 240−340 of the P22 subunit may represent a conserved evolutionary domain of importance in DNA translocating functions. Basic side chains of the P22 portal subunit are also clustered within the same sequence, further suggesting a possible role in DNA translocation.

Insights into the subunit structure and molecular mechanism of assembly of the P22 portal protein have been obtained by Raman spectroscopy (*13*) of a biologically active recombinant form (*6*, *14*). The monomeric portal subunit exhibits an α/β fold that is dominated by α-helix. Although the monomer conformation is largely conserved upon dodecamer assembly, appreciable changes are apparent in Raman markers that report on the local environments and interactions of subunit side chains. Extensive changes in side-chain environments without appreciable changes in secondary structure may reflect a supramolecular organization process that exploits hinge-like motions of preformed domains rather than plasticity throughout the subunit structure. Such a Raman perturbation signature has been considered characteristic of strong protein/protein interactions (*9*, *13*, *21*). Conspicuous among the subunit side chains altered by portal protein dodecamerization are the cysteines (Cys 153, Cys 173, Cys 283, and Cys 516), which undergo a major reorganization in their S−H···X hydrogen-bonding states. One cysteine of the P22 portal subunit — Cys 283 — falls within the above-noted domain (residues 240−340) putatively conserved with the φ29 portal subunit.

To further characterize the roles of Cys 283 and other cysteines of the P22 portal subunit in folding and dodecamer assembly pathways, we employed site-directed mutagenesis to construct the four single-site Cys → Ser mutants for biophysical analyses. Here, we report the results of investigations by size-exclusion chromatography and Raman difference spectroscopy. We note that a recent investigation of single-site Cys → Ser mutants of the trimeric tailspike of phage P22 demonstrated five different Raman sulfhydryl markers comprising seven distinct sulfhydryl hydrogen-bonding states for the eight cysteines per tailspike subunit (*11*). A subset of the eight tailspike cysteines is crucial to the folding and assembly pathway of the native trimer. The profile of cysteine signatures of the P22 portal protein, although less complex than that of the tailspike protein, is nevertheless also demonstrably sensitive to the assembly pathway (*13*). At least one portal cysteine (Cys 283) falls within a domain that may function in DNA translocation. The present results identify a distinct Raman S−H marker and a specific hydrogen-bonding state for each of the four cysteine sulfhydryls of the P22 portal protein in both monomeric and assembled states and correlate the cysteine hydrogen-bonding environments with subunit folding and assembly. The findings demonstrate that P22 portal cysteines, like the tailspike cysteines, can manifest unexpected and diverse roles in protein maturation pathways.

EXPERIMENTAL PROCEDURES

Site-Directed Mutagenesis of the Portal Protein Gene. Plasmids for expression of recombinant portal proteins were constructed using the polymerase chain reaction (PCR). The fidelity of each amplified DNA sequence was confirmed by standard methods (*22*). The following primers (mutations underlined) were designed in accordance with the requirements of the ExSite PCR-Based Site-Directed Mutagenesis Kit (Stratagene, La Jolla, CA): (*i*) 5′-CCT CCT CCC ATG TTA TCT GG and 5′-CAC TAT GGA TAG GCT CTC GAC for the C153S mutant; (*ii*) 5′-CAC TCC ACA GTT ATC CAC TCA ATG AGC and 5′-ACG GGC GTC AGA CTT ATC CAT C for C173S; (*iii*) 5′-TCC ACT GCT GTA CTC AAA GAC AAG and 5′-GGT GAT AAT CGA TTT GTA TAC TAC CCG for C283S; (*iv*) 5′-TCC TAC ACG GAT GTT GGA CCA T and 5′-CTC ATA GCG CCC CCT GAT ATC GTT for C516S. Primers were synthesized by Integrated DNA Technologies, Inc. (Coralville, IA) and were purified by polyacrylamide gel electrophoresis (PAGE) before use in mutagenesis reactions. The double-stranded DNA template for wild-type (WT) gene *1* was a gift from Prof. Peter E. Prevelige, Jr., University of Alabama, Birmingham (*6*). This pseudo-wild-type plasmid, denoted pET-g1a (7617 bp), was found to contain a heretofore unreported base mutation (T1816C) that leads to replacement of proline by serine at position 606 in the portal protein sequence. The plasmid was also constructed with a His_6 tag to facilitate purification (*6*, *23*). Each of the above four pairs of primers was annealed to the parent pET-g1a plasmid to generate by PCR the four single-site Cys → Ser mutant plasmids, designated pET-g1aC153S, pET-g1aC173S, pET-g1aC283S, and pET-g1aC516S. PCR products were analyzed by stan-

dard agarose gel electrophoresis using appropriate size markers to verify the integrity of the PCR products. Once ligated into the vector, the PCR products were transformed into *E. coli* XL1-Blue supercompetent cells (Stratagene, La Jolla, CA).

To confirm the correct inserts, the plasmids were amplified in *E. coli* XL1-Blue, purified with a commercially available kit (Qiagen, Inc., Valencia, CA), and digested with the appropriate restriction enzymes (*Xho I* and *Xba I*). The digests were analyzed on 0.8% agarose gels prepared in Tris-acetate-EDTA buffer (40 mM Tris-acetate, 2 mM EDTA, pH 7.5). DNA samples were diluted 10-fold in the loading buffer (20% Ficoll 400, 100 mM EDTA, pH 8.0, 1% SDS, 0.25% bromophenol blue, 0.25% xylene cyanol). The mutated portal gene of each plasmid was also verified directly by sequence determination (Lone Star Labs, Houston, TX).

Expression, Purification, and In Vitro Assembly of Mutant Portal Proteins. The mutated portal genes were transformed into *Escherichia coli* BL21-Gold(DE3) (Stratagene, La Jolla, CA) and overexpressed as previously described for the WT plasmid (*6*). The cells were grown at 37 °C to $OD_{600} = 0.7$ in LB medium containing 100 μg/mL ampicillin, then shifted to 28 °C and induced with 1 mM IPTG for 5 h. The cells were harvested by centrifugation and resuspended in 1/20 volume cold nickel binding buffer (20 mM imidazole, 500 mM NaCl, 20 mM TrisHCl, pH 7.9) to which lysozyme was added to a final concentration of 0.1 mg/mL. Two protease inhibitor tablets (EDTA-free Mini Protease Inhibitor cocktail, Boehringer Mannheim, Indianapolis, IN) were added to the cells, and the suspension was placed on ice and allowed to lyse. The lysate was sonicated to reduce viscosity and pelleted at 1000 S. Each mutant was purified at 4 °C by Ni-affinity chromatography (5 mL HiTrap chelating column, Amersham Pharmacia Biotech, Piscataway, NJ) and eluted with 500 mM imidazole. The protein was demonstrated to be free of degradation products or contaminating proteins by SDS−PAGE. A final concentration of 10 mM EDTA was needed to maintain protein solubility in the elution buffer. The monomeric portal protein was separated from oligomeric forms by anion-exchange chromatography using two 5 mL HiTrap Q columns in series (Amersham Pharmacia Biotech, Piscataway, NJ) as previously described (*6*). Each purified monomer was eluted with 240 mM NaCl, 2 mM EDTA, 30 mM TrisHCl, pH 7.5, diluted to a concentration of 0.5 μg/μL or less in 100 mM NaCl, 2 mM EDTA, 10 mM TrisHCl, pH 7.5 (buffer A), and stored at −80 °C. Purified mutant proteins were analyzed by MALDI−TOF (Voyager-De-Pro, Applied Biosystems, Foster City, CA) and electrospray mass spectrometry (LCQ, Thermo Finnigan, San Jose, CA) to confirm molecular mass. Protein concentrations were determined by UV absorption spectrophotometry (Cary model 3E, Varian, Palo Alto, CA) of samples denatured in 6.0 M guanidinium chloride using the molar extinction (ϵ_{280} = 99 740 M^{-1} cm^{-1}) calculated for the denatured protein in (*24*).

The purified mutant portal proteins were treated using the same procedure established previously to oligomerize the WT subunit (*6*). This involved incubation of a moderately concentrated solution (50 μg/μL) for 24 h at 25 °C. The mutant portal oligomers so obtained were purified on HiTrap Q anion-exchange columns. The fraction eluted with 660 mM NaCl, 2 mM EDTA, 30 mM TrisHCl, pH 7.5, was diluted to buffer A and stored at −20 °C.

Size-Exclusion Chromatography. Analytical high performance size exclusion chromatography (HPSEC) with a 280 nm wavelength detector (ÄKTA system, Amersham Pharmacia Biotech, Piscataway, NJ) was employed to compare time-dependent changes in the state of aggregation of mutant proteins. Gel filtration of each purified protein was performed using a 300SW column (Waters, Milford, MA) equilibrated in buffer A. The column was run at 4 °C with a flow-rate of 0.75 mL/min. The proteins for HPSEC analysis were diluted to 0.1 μg/μL in buffer A from stock solutions prepared at the same concentrations employed for Raman experiments (∼35 μg/μL, see below). The HPSEC data for kinetics analysis were obtained over a 60 h period on both WT and mutant subunits. Distributions of portal protein between monomeric and oligomeric states as a function of time were determined from the areas of corresponding HPSEC peaks.

Electron Microscopy. Portal rings assembled in vitro were diluted to 0.05 μg/μL and adhered to carbon-coated copper grids. Samples were blotted to remove excess material, fixed for 1 min with 1.0% formaldehyde, and stained for 20 s with 2% uranyl acetate solution. Micrographs of the stained samples were obtained on a model 1200EX Mark II electron microscope (JEOL USA, Inc., Peabody, MA) and recorded on Kodak SO163 film at 60 000× magnification using an objective lens defocus of ∼1.0 μm and estimated electron dose of 20 $e^-/Å^2$.

Raman Spectroscopy. Stock solutions of monomeric and oligomeric portals were thawed, separated from storage buffer using a Centricon-50 device (Amicon, Danvers, MA) with 50-kDa cutoff, and brought to 35 μg/μL in buffer A for Raman spectroscopy. Amide I and amide III Raman markers of mutant subunit secondary structure were found to be concentration independent in the range of 25−100 μg/μL, as noted previously for the WT protein (*13*). Proteins were also assessed by HPSEC both before and after Raman spectral data collections to confirm retention of protein integrity. Typically, a 5-μL aliquot of each protein solution was transferred to a 1.0-mm glass capillary tube (Kimax no. 34502), which was sealed immediately prior to data collection.

Raman spectra were excited with ∼30 mW of 532-nm radiation from a frequency-doubled Nd:YAG laser (Verdi, Coherent Inc., Santa Clara, CA) and collected on a single spectrograph (model 500M, SPEX Ind., Edison, NJ) equipped with a holographic notch filter, holographic grating, and liquid-nitrogen cooled, charge-coupled-device detector. Samples were thermostated at 4 °C during data collection protocols. Further details of the instrumentation have been described (*25*).

RESULTS

Portal Clones Exhibit Gene 1 Mutations that Encode Single-Site Cys → Ser Substitutions. The four plasmids required for recombinant expression of the single-site Cys → Ser mutant portals were constructed using the ExSite PCR-Based Site-Directed Mutagenesis Kit, as described in Experimental Procedures. Each PCR amplification product was analyzed by agarose gel electrophoresis and shown to consist of a single band corresponding to a 7617-bp plasmid. Each mutant plasmid was also sequenced in entirety to verify the expected Cys → Ser codon substitution (sequences available from the authors on request).

Cultures of His-tagged mutant portals were grown at 28 °C to minimize possible oligomerization reactions of the expression product (*6*). SDS gels indicated comparable levels of expression of WT and mutant portals as a function of time following IPTG induction. (Further details of gel electrophoresis are described at the laboratory web site, http://sbs.umkc.edu/gjthomas-lab/protocols/index.html.) Following cell lysis and centrifugation, each soluble mutant was separated from the supernatant using the same Ni-column chromatographic procedure described previously for the WT protein (*6*, *13*). Yields of these initially purified mutants were comparable to the WT yield, as judged from Ni-affinity column chromatograms. Subsequent anion exchange (Q-column) chromatography to separate the monomeric mutant from soluble oligomeric forms generally yielded less than 60% of the monomer recovery of WT portal protein. MALDI−TOF and electrospray mass spectra were obtained on each portal mutant to verify that the protein mass corresponded to a single-site Cys → Ser substitution.

The majority of each purified mutant yield consisted of apparently non-native soluble material, which was discarded. In typical separation protocols of 4-h duration, yields of the desired mutant monomers were C153S (3 mg), C173S (2 mg), C283S (7 mg), and C516S (2 mg) per 100 mL of culture. Conversely, 12−15 mg of WT monomer could be purified per 100 mL of culture. These results suggest that C283S forms the most stable mutant monomer (∼50% of WT recovery), whereas all other mutants form somewhat less stable monomers (∼20% of WT recovery). Nevertheless, single-site Cys → Ser mutants of the P22 portal protein were more efficiently recovered than Cys → Ser mutant variants of the P22 tailspike protein (*10*).

Portal Assembly Is Significantly Affected by Cys → Ser Mutations. Monomeric and dodecameric forms of the P22 WT portal protein are readily distinguished by their characteristic elution times using HPSEC, as indicated in Figure 2A. The data shown correspond to 60−72 h incubations of a 50 μg/μL solution of purified protein at 4 °C (i.e., the same sample concentration and temperature employed for Raman spectroscopy). The intense elution peaks at 8 and 10 min correspond to the portal protein dodecamer and monomer, respectively. The much weaker elution peak at 15 min is attributed to a small fraction of monomeric portal that undergoes apparent proteolysis at these experimental conditions (*6*, *13*). On the basis of the elution peak intensities, the uncharacterized fragment represents only about 2% of the sample, while the monomer and dodecamer represent about 48 and 50% of the total, respectively. The data indicate a relatively long half-life for assembly of the WT monomer ($t_{1/2}^{WT}$ ∼60 h) at these in vitro conditions. Figure 2B shows the distribution (based upon HPSEC elution peak intensities) of WT portal between monomer and oligomer states as a function of time over a 60-h period. The results demonstrate that the depletion of monomer corresponds directly to the accretion of dodecamer and that the proteolytic event becomes insignificant as the portal monomer population decreases. Identical HPSEC analyses (data not shown) were performed for mutant portal proteins at the same experimental conditions.

Figure 2C,D compares monomer/dodecamer distribution profiles of WT and mutant portals as a function of time of incubation of 50 μg/μL solutions at 4 °C. The data

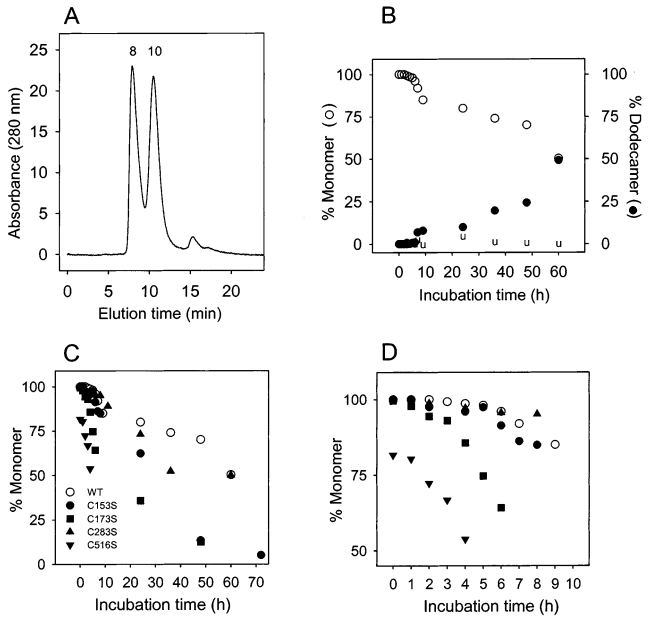

FIGURE 2: Characterization by HPSEC of portal protein monomer-to-oligomer distributions in the 50 μg/μL solutions examined by Raman spectroscopy (see also Figure 4, below). Panel A: HPSEC chromatogram of the WT portal subunit after incubation of a 50 μg/μL solution at 4 °C for 60 h. Band areas of the fractions eluting at 10 min (monomer) and 8 min (oligomer) indicate an approximately equal monomer-to-oligomer distribution at these conditions. Panel B: Plots showing the monomer (left ordinate) and dodecamer (right ordinate) distributions of WT portal protein vs time of incubation at 4 °C. Panel C: Plots of the monomer/oligomer distributions of portal protein variants (WT ○, C153S ●, C173S ■, C283S ▲, and C516S ▼) vs time of incubation (0−70 h) at 4 °C. Panel D: Amplification of the 0−10 h interval of panel C. All samples were chromatographed after dilution of a 50 μg/μL solution to 0.1 μg/μL in buffer A.

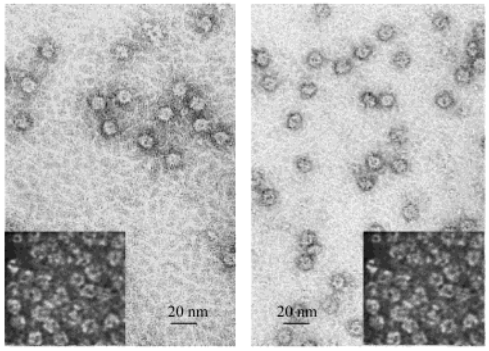

FIGURE 3: Negative-stain electron micrographs of oligomeric portal proteins obtained at 60 h after elution by HPSEC (see Figure 2). The ring assemblies formed by C153S (left) and C516S (right) mutants are similar in size and shape to the WT portal (inset of each panel). C173S and C283S could not be visualized as portal-like rings by EM.

demonstrate distinctive assembly kinetics for each portal variant. For example, the half-life of the C153S monomer population ($t_{1/2}^{C153S}$ ∼30 h) is a factor of 2 lower than that observed for the WT protein. The corresponding rate of growth of the C153S oligomer population (data not shown) is more rapid than that of WT oligomerization. The left panel of Figure 3 shows a negative stain electron micrograph of the oligomeric particles formed by C153S. At this resolution, the C153S mutant portal is morphologically indistinguishable from the WT portal (cf. inset). We conclude that the C153S mutant portal protein is competent to assemble into portal-

Table 1: Assembly Characteristics of Wild-Type and Mutant (Cys → Ser) Portal Proteins[a]

	WT	C153S	C173S	C283S	C516S
$t_{10\%}{}^{4\,°C}$ (h)	10	6	3	11	(0)
$t_{1/2}{}^{4\,°C}$ (h)	60	30	20	36	5
proteolysis	no	no	yes	yes	no
oligomerization	yes	yes	yes	yes	yes
monomer	stable	stable	unstable	hyperstable	unstable
oligomer	stable	stable	unstable	stable	stable
ring formation	yes	yes	?	no	yes

[a] Stabilities are compared on the basis of the times in hours required for 10% ($t_{10\%}{}^{4\,°C}$) and 50% ($t_{1/2}{}^{4\,°C}$) depletion of initial monomer populations as judged from the HPSEC data discussed in the text. Proteolysis implies conversion of more than 10% of the monomer to lower molecular weight species with ~15 min. Ring formation is based upon visualization by negative stain electron microscopy.

like dodecamers, which are stable for several days.

Figure 2C shows that the C173S monomer population also diminishes very rapidly, descending to 60% of the initial population within 5 h. Although the HPSEC elution time observed for the C173S oligomer (peak at 10.5 min, data not shown) corresponds closely to that of the WT portal dodecamer (Figure 2A), no ring-like particles could be observed by electron microscopy (EM). These results suggest that although the C173S portal protein is competent to oligomerize into ring-like dodecamers, such assemblies are not as stable as WT portals and apparently undergo either off-pathway aggregation or disassembly that precludes EM visualization within the time frame of the experiments (~60 h). This is consistent with time-dependent changes observed also in Raman spectra of the C173S assemblies (below).

Unlike the C153S and C173S mutant portals, the C283S mutant shows little difference from WT in monomer stability during the first 24 h of incubation at 4 °C (Figure 2C). After 24 h, however, the monomer population falls more rapidly, and the corresponding oligomer population rises more rapidly than WT ($t_{1/2}{}^{C283S}$ ~36 h). For example, at 36 h, ~50% of C283S (as compared with ~20% of WT protein) exists as oligomer. Surprisingly, for $t > 36$ h, we observe no further increase in oligomer population and no further decrease in monomer population, suggesting that the remaining monomer is not competent to oligomerize after 36 h of incubation (data not shown). Because no significant fragmentation of monomers is observed after 36 h, the termination of assembly may be due to an intramolecular conformational rearrangement or to a critical concentration threshold for oligomerization that is higher than for WT. The initial slow depletion of the C283S monomer population favors Raman investigation of this mutant in the monomeric state. Like C173S, a ring-like structure of C283S could not be observed by EM.

The C516S mutant, which exhibits $t_{1/2}{}^{C516S}$ ~5 h, is the least stable mutant monomer (Figure 2C). Nevertheless, C516S readily forms very stable oligomers, and these are well-visualized as portal-like rings by EM (Figure 3). The rapid ring formation of C516S at 50 μg/μL and 4 °C disfavors Raman spectroscopic examination of the monomer. A summary of HPSEC and EM results on WT and mutant portals is given in Table 1.

Raman Signatures of Mutant Portal Proteins. 1. Monomeric State. Effects of Cys → Ser mutations on portal protein structure were probed by Raman spectroscopy. Solution samples of C153S, C173S, C283S, and C516S were prepared as described in Experimental Procedures, and spectral data were collected within 30 min after solution preparations to ensure that the proteins remained predominantly monomeric. In the cases of C173S and C516S, which exhibit enhanced oligomerization kinetics (Figure 2), the spectral data were obtained from ~20 μg/μL solutions to disfavor the oligomerizations promoted at higher concentrations as evidenced by HPSEC. Raman spectra (600−1800 cm^{-1}) of WT and representative mutant (C153S and C283S) monomers are compared in the left panel of Figure 4. Digital difference spectra computed between mutant and WT portal monomers are shown in the lower traces of the panel. The absence of appreciable differences indicates that secondary and tertiary structures of the native WT monomer are largely conserved with the single-site Cys → Ser substitutions. Comparable data (not shown) were also obtained for C173S and C516S. In every case, a small positive difference feature at 1665 cm^{-1} is observed for the Raman amide I band, which suggests a slight excess of non-native β-stranded structure in the mutant. The difference feature is largest for C173S (~5% of the integrated amide I intensity) and may represent the formation of a small population of off-pathway aggregates (*13*). Cys and Ser side chains do not contribute significantly to the 600−1800 cm^{-1} region of the protein Raman signature (*11*, *26*).

Cysteine Raman markers of the portal proteins occur in the 2520−2600 cm^{-1} interval of the Raman spectrum (*13*). Such bands originate from S−H stretching vibrations and are diagnostic of cysteine S−H···X hydrogen-bonding environments (*27*). The Raman S−H signatures of the mutant and WT portal monomers are compared in Figure 5A (left panel). Corresponding difference spectra of Figure 5A (right panel), computed as mutant-minus-WT, exhibit negative intensity that identifies the S−H marker eliminated or diminished by each Cys → Ser mutation. The data of Figure 5A resolve the residue-specific Raman sulfhydryl band assignments and provide an internally consistent S−H···X classification scheme for the portal monomers, as summarized in the middle section of Table 2. The results show that the composite S−H Raman band envelope of the WT monomer comprises the following: (i) moderate S−H···X interactions from Cys 173 and Cys 283 and (ii) strong S−H···X interactions from Cys 153 and Cys 516. It is surprising that neither the C153S nor the C516S mutation is refractory to ring formation, although each mutation eliminates a robust S−H···X hydrogen bond of the portal monomer.

We also find that the sum (not shown) of cysteine Raman signatures of monomeric mutant portals closely approximates the Raman S−H profile of the WT monomer. This suggests that in each mutant portal monomer the replacement of a cysteine side chain by a serine has no significant effect upon the hydrogen-bonding state of any other cysteine side chain.

2. Assembled State. Raman spectra were also obtained on the portal mutants at conditions favorable to the formation of dodecameric rings (Figure 2) to assess the effects of the mutations on subunit secondary and tertiary structures (600−1800 cm^{-1} region) and on S−H···X environments (2520−2600 cm^{-1}) in the portal assemblies. Raman spectra (600−1800 cm^{-1}) of WT and representative mutant (C153S and C283S) oligomers are compared in the right panel of Figure 4. Digital difference spectra computed between mutant and WT oligomers are shown in the lower traces of the panel.

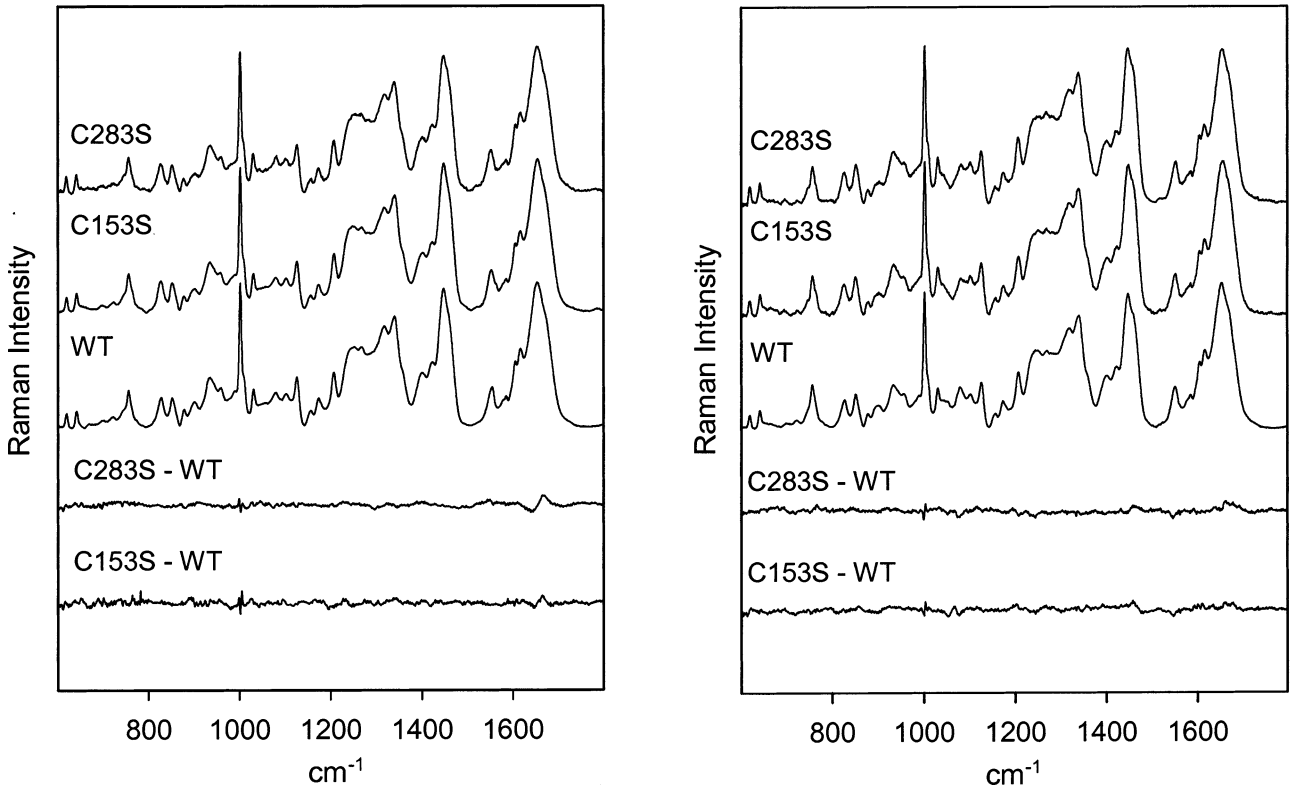

FIGURE 4: Raman spectra (600−1800 cm^{-1}) of WT and mutant portal proteins. Left panel: Raman spectra of monomeric forms of WT, C153S, and C283S portal proteins, as labeled. The lower two traces compare the corresponding Raman difference spectra, computed as mutant-minus-WT. Right panel: Raman spectra of oligomeric forms of WT, C153S, and C283S portal proteins, as labeled. The lower two traces compare the corresponding Raman difference spectra, computed as mutant-minus-WT. Spectra were excited at 532 nm from aqueous samples maintained at 4 °C (see text). The typical spectral acquisition time was 10 min (average of five files each consisting of four accumulations of 30 s).

The data show that secondary and tertiary structures of the mutant assemblies are indistinguishable from those of the WT dodecamer. Comparable data (not shown) were also obtained for C173 and C516S.

We also compared by digital difference the Raman spectrum of each mutant oligomer with that of its monomer (data not shown). The results were in accord with those reported previously for the WT portal protein (*13*), viz. very small changes in Raman amide bands but significant changes in side chain Raman markers indicating perturbations of subunit interfaces without appreciable change in subunit secondary structure.

Cysteine Raman signatures (2520−2600 cm^{-1}) of the mutant and WT assemblies are shown in the left panel of Figure 5B and are compared as mutant-minus-WT differences in the right panel of Figure 5B. Several patterns can be identified from the data: (i) Each portal variant exhibits a Raman S−H signature that is greatly perturbed by assembly. (A detailed discussion of the effects of assembly on the wild-type S−H···X signature has been given previously (*13*).) (ii) All assemblies exhibit a Raman peak at 2570 cm^{-1} or higher, despite the absence of such a marker in the monomeric form. This indicates that in every mutant, as well as in WT, at least one Cys S−H group is transferred from a stronger to a weaker S−H···X hydrogen-bonding state. (iii) With the exception of C516S, no mutant exhibits an S−H group that is promoted to a stronger hydrogen-bonding state with assembly. Surprisingly, the two mutant variants that form WT-like rings visualized by EM (i.e., C153S and C516S (Figure 3)) also produce the most distinctive Raman S−H differences vis-à-vis WT.

The difference spectra computed between mutant and WT assemblies are complex. In previous work on Cys → Ser mutant tailspikes of phage P22, Raso et al. (*11*) were able to deduce the unique S−H signatures of all eight cysteines of the WT tailspike. The tailspike Raman data indicated that Cys signatures are uncoupled to one another (i.e., mutation of one Cys site does not perturb the S−H···X hydrogen-bonding state of any other Cys site (*11*)). While Figure 5A shows this to be true also for the portal monomers, Figure 5B indicates that cysteine signatures of the assemblies are not similarly conserved. A tabulation of plausible assignments and S−H···X hydrogen-bonding schemes for the mutant portal assemblies is given in the right column of Table 2.

3. Effect of Assembly on the Raman S−H Signature of Each Cys → Ser Mutant. Assembly of the WT portal subunit into a dodecameric ring has little effect upon the protein secondary structure but greatly perturbs the local environments of specific side chains, including cysteines (*13*). To assess the effects of assembly on the Raman S−H signature of each Cys → Ser mutant and to compare the results with the WT portal, we computed the difference spectrum between the assembled and the monomeric states of each portal variant, as shown in the left panel of Figure 5C. The data suggest complex patterns of S−H···X interactions in the portal assemblies. An unexpected finding is that the sum of spectra of mutant assemblies cannot be scaled to accurately

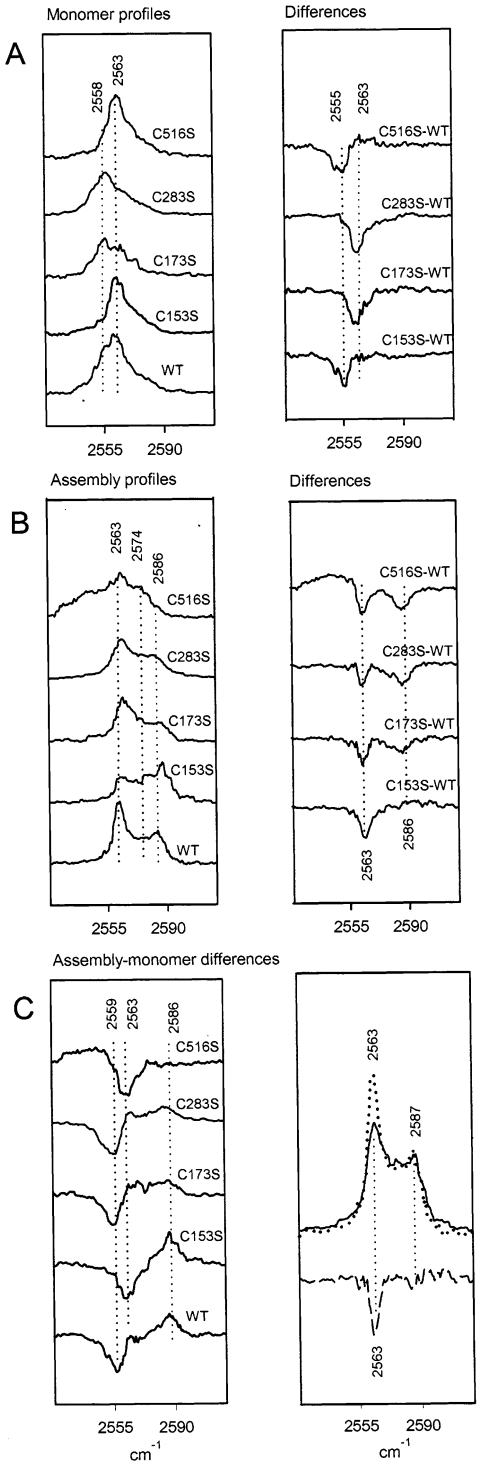

FIGURE 5: Raman profiles of WT and mutant portal proteins in the region of cysteine S−H stretching vibrations (2520−2620 cm^{-1}). The typical spectral acquisition time for each of these traces was 30 min (average of five files each consisting of four accumulations of 90 s). Other conditions are as given in Figure 4. (A) The left panel compares S−H profiles of the monomeric proteins (WT and mutants, as labeled). The right panel shows the S−H signature specific to each cysteine of the WT monomer, obtained by subtracting the WT spectrum from the corresponding mutant spectrum. (B) The left panel compares S−H profiles of the assembled proteins (WT and mutants, as labeled). The right panel shows the S−H signature specific to each cysteine of the WT assembly, obtained by subtracting the WT spectrum from the corresponding mutant spectrum. (C) The left panel shows the computed assembly-minus-monomer difference spectrum for each variant, as labeled. The right panel demonstrates the nonadditivity of cysteine signatures for the assembled proteins. Thus, the Raman signature of C516 that is obtained by subtracting the C516S mutant spectrum from the WT spectrum (panel B, top right) is not identical to the C516 signature (dashed-line trace) generated by subtracting the sum of signatures of C153, C173, and C283 (solid line trace) from the WT spectrum (dotted line trace).

Table 2: Sulfhydryl Raman Markers and S−H···X Hydrogen-Bond Strengths of Portal Cysteines[a]

	monomeric form		assembled form	
cysteine[b]	cm^{-1}	H-bond	cm^{-1}	H-bond
Cys 153	2558[c]	strong	2563[c]	moderate
Cys 173	2563[c]	moderate	2563[d] (50%)	moderate
			2586[d] (50%)	very weak
Cys 283	2563[c]	moderate	2563[d] (27%)	moderate
			2586[d] (73%)	very weak
Cys 516	2558[c]	strong	2563 (50%)	moderate
			2586 (50%)	very weak

[a] Hydrogen-bond strengths of SH donors are based upon model compound studies of Li and Thomas (*27*), which discriminate strong (2550−2560 cm^{-1}), moderate (2560−2575 cm^{-1}), weak (2575−2580 cm^{-1}), and very weak (2580−2585 cm^{-1}) bonds involving O, N, and S acceptors. [b] Amino acid residue in wild-type portal protein. [c] Peak of the Raman S−H stretching band. [d] Component of closely spaced doublet; the percentage of the total Raman intensity contributed by each component of the doublet is given in parentheses.

represent the WT spectrum, which indicates the likelihood in one or more mutants of coupling between SH environments. This is illustrated in the right panel of Figure 5C, where the WT cysteinyl spectrum (dotted-line trace) is subtracted from the spectral sum, C153 + C173 + C283 (solid-line trace), to generate an inversion of the expected C516 signature (broken-line trace). This expected C516 signature shows a single sharp trough at 2563 cm^{-1} in lieu of the two troughs at 2563 and 2586 cm^{-1} (Figure 5B, right panel, top trace), which are obtained upon direct subtraction of WT from C516S. If no coupling of Cys environments occurred, the two differences would be identical. Nonadditivity of the portal Cys → Ser mutant spectra contrasts with the results reported previously for Cys → Ser mutants of the P22 tailspike assembly (*11*).

DISCUSSION AND CONCLUSIONS

The monomeric subunit of the P22 portal contains four cysteines—Cys 153, Cys 173, Cys 283, and Cys 516—all of which are reduced and vulnerable to deuterium exchange at physiological conditions. In the native dodecamer that is competent for incorporation into the procapsid, the cysteine sulfhydryls remain reduced and are distributed equally between weak and strong S−H···X hydrogen-bonding environments. Two of the four SH groups per subunit become protected from deuterium exchange in the dodecamer assembly (*13*). To identify the sulfhydryl Raman signature of each cysteine and to further assess the roles of S−H···X interactions in portal ring formation, we have engineered single-site Cys → Ser mutant portal proteins and obtained and interpreted their Raman spectra in both monomeric and assembled states.

A precedent for Raman characterization of cysteine SH environment and S−H···X interaction in protein folding and assembly is the P22 tailspike trimer (*11*). Single-site Cys → Ser substitutions in the tailspike protein do not absolutely prevent expression, folding, or assembly, although distinct defects in folding kinetics and trimerization efficiencies can be identified for each mutant. Once assembled, however, each mutant tailspike exhibits nativelike secondary structure, thermostability, SDS resistance, and biological activity (*10*). The present results show that cysteines of the P22 portal subunit define a different class of protein sulfhydryl interac-

tions: With only one exception (C153S), the Cys → Ser mutations of the portal protein have a significant impact on in vitro stability, nativelike ring formation, or assembly pathway. Small but measurable changes (<5%) in monomer secondary structure are also detected. Furthermore, in the case of C516S, the environments of the remaining nonmutated cysteines appear to be collectively affected by the point mutation at residue 516.

All four Cys → Ser mutant portals have distinct phenotypes. C153S exhibits physical properties that are closest to those of the wild-type portal, including similar monomer stability (HPSEC), ring morphology (EM), and subunit fold (Raman spectroscopic signatures). We conclude that sulfhydryl interactions of Cys 153 are not essential to subunit folding or assembly and that the SH group of Cys 153 in the mature assembly does not play a critical structural role at the intersubunit interface. Viability of the Ser 153 portal mutant is supported by the fact that the related dsDNA bacteriophage HK620 (portal protein of 708 aa with 32% sequence homology to the P22 portal protein) contains Ser at the corresponding amino acid site (*28*). We speculate that mutations other than Cys → Ser at site 153 of the P22 portal subunit also would be favorable to portal assembly and function. This is suggested by the substitution of Ala for Cys at the 153 site in the portal protein of the related dsDNA phage ASPE-1 (720 aa, 31% sequence homology with P22) (*28*).

The mutant C173S, which is highly unstable as compared to the wild-type monomer, does not assemble efficiently into rings, undergoes proteolytic cleavage, and appears to form an off-pathway aggregate. We infer that the highly polar seryl OH group in lieu of the weakly polar cysteinyl SH group at position 173 precludes a stable monomer fold. Consistent with this conclusion is the occurrence of the nonpolar alanyl side chain at the equivalent site in the portals of phages HK620 and ASPE-1 (*28*).

The mutation C283S results in a strikingly hyperstable monomeric portal, which resists ring assembly in the same time interval that allows efficient dodecamerization of the WT protein. This may reflect strong seryl $O^{\gamma}-H\cdots X$ or $H\cdots O^{\gamma}-H$ hydrogen bonding with protein sites or solvent in lieu of weaker $S-H\cdots X$ interaction in the wild-type monomer. Such seryl interactions may prevent or interfere with productive intersubunit association. Alternatively, cysteine at position 283 may be important for α-helix capping. Cysteinyl side-chain capping interactions are known to stabilize many native protein folds (*29*). Cys 283 is the only cysteine located within the fold that is thought to constitute a domain common to both P22 and ϕ29 portal subunits (*13*, *17*). In ϕ29, this fold lines the DNA translocating channel; a similar function is presumably fulfilled by the corresponding fold in P22. Interestingly, Cys 283 is preceded by a string of highly basic residues ($KRRR^{275}$) that may participate in DNA interaction. Thus, Cys 283 has the potential not only for α-helix capping but also for influencing the interface of the DNA translocating channel. The defect of the C283S mutant monomer suggests a role for Cys 283 in portal activity.

The mutant C516S rapidly forms oligomers (Figure 2), which are easily visualized by EM as portal-like rings (Figure 3). The Raman S−H profile of the C516S assembly indicates significant perturbations to $S-H\cdots X$ interactions of one or more nonmutated cysteine sites (Figure 5). (Such coupling is not observed for the monomeric state of C516S, as noted above.) Coupling of S−H interactions was not detected in previously examined Cys → Ser mutants of the P22 tailspike protein (*11*). The present observations suggest an assembly related rearrangement of portal tertiary structure without significant impairment of intersubunit recognition.

We have noted that the most robust $S-H\cdots X$ hydrogen bonds of the portal monomer are contributed by the sulfhydryls of Cys 153 and Cys 516 (right panel of Figure 5A). Cys → Ser mutation at either 153 or 516, which presumably results in the replacement of a native-state strong $S-H\cdots X$ interaction by a correspondingly strong $O^{\gamma}-H\cdots X$ hydrogen bond, has no deleterious effect on portal assembly. We conclude that strong hydrogen bonding by the 153 and 516 side-chain donor groups stabilize a particular monomer conformation that is competent in dodecamer assembly. On the other hand, native portal assembly apparently requires weaker hydrogen-bonding interactions from the Cys 283 and Cys 173 side chains. The Cys 283 → Ser and Cys 173 → Ser mutations, which introduce strongly hydrogen-bonding $O^{\gamma}H$ groups, are more highly detrimental to portal assembly.

The present findings underscore important roles for cysteines in the efficiency of portal protein folding and assembly. Single-site Cys → Ser mutations of the P22 portal subunit, like those of the P22 tailspike subunit (*10*), reveal a wide range of hydrogen-bonding environments for the sulfhydryl moiety and show that the local environment of each cysteine sulfhydryl is impacted by assembly. Substitution of a single $O^{\gamma}-H\cdots X$ interaction for an $S-H\cdots X$ interaction in the portal subunit can perturb secondary and tertiary structures, decrease or increase the rate of quaternary structure formation, or promote off-pathway aggregation, depending upon the sequence and structure context. Remarkably, two of the cysteines of the P22 portal protein (Cys 173 and Cys 283) yield Raman band doublets rather than the expected singlets diagnostic of a single hydrogen-bonding partner. Doublets were also observed for a subset of tailspike cysteines (Cys 267 and Cys 287) (*11*). The Raman S−H doublet is evidence that the cysteine sulfhydryl in question is distributed between two hydrogen-bonding acceptors in the native structure. The similar results obtained on P22 portal and tailspike proteins suggest that multiple hydrogen-bonding partners for a given cysteine sulfhydryl may not be an uncommon molecular mechanism for protein structure stabilization.

ACKNOWLEDGMENT

A.R.-C. thanks Dr. W. Kelly Thomas (University of New Hampshire) for guidance in the design and expression of mutants. We also thank Drs. Peter E. Prevelige, Jr. (University of Alabama at Birmingham), Stacy A. Overman (UMKC), and James M. Benevides (UMKC) for helpful discussions and constructive comments on the manuscript.

REFERENCES

1. Casjens, S., and King, J. (1975) Virus assembly, *Annu. Rev. Biochem. 44*, 555−611.
2. Prevelige, P. E., Jr., and King, J. (1993) Assembly of bacteriophage P22: A model for ds-DNA virus assembly, *Prog. Med. Virol. 40*, 206−221.
3. Greene, B., and King, J. (1999) Refolding and stability of mutant scaffolding proteins defective in P22 capsid assembly, *J. Biol. Chem. 274*, 16141−16146.

4. Zhang, Z., Greene, B., Thuman-Commike, P. A., Jakana, J., Prevelige, P. E., Jr., King, J., and Chiu, W. (2000) Visualization of the maturation transition in bacteriophage P22 by electron cryomicroscopy, *J. Mol. Biol. 297*, 615−626.
5. Tuma, R., Tsuruta, H., Benevides, J. M., Prevelige, P. E., Jr., and Thomas, G. J., Jr. (2001) Characterization of subunit structural changes accompanying assembly of the bacteriophage P22 procapsid, *Biochemistry 40*, 665−674.
6. Moore, S. D., and Prevelige, P. E., Jr. (2001) Structural transformations accompanying the assembly of bacteriophage P22 portal protein rings in vitro, *J. Biol. Chem. 276*, 6779−6788.
7. Teschke, C. M., and King, J. (1993) Folding of the phage P22 coat protein in vitro, *Biochemistry 32*, 10839−10847.
8. Tuma, R., Prevelige, P. E., Jr., and Thomas, G. J., Jr. (1996) Structural transitions in the scaffolding and coat proteins of P22 virus during assembly and disassembly, *Biochemistry 35*, 4619−4627.
9. Tuma, R., Prevelige, P. E., Jr., and Thomas, G. J., Jr. (1998) Mechanism of capsid maturation in a double-stranded DNA virus, *Proc. Natl. Acad. Sci. U.S.A. 95*, 9885−9890.
10. Haase-Pettingell, C., Betts, S., Raso, S. W., Stuart, L., Robinson, A., and King, J. (2001) Role for cysteine residues in the in vivo folding and assembly of the phage P22 tailspike, *Protein Sci. 10*, 397−410.
11. Raso, S. W., Clark, P. L., Haase-Pettingell, C., King, J., and Thomas, G. J., Jr. (2001) Distinct cysteine sulfhydryl environments detected by analysis of Raman S−H markers of Cys → Ser mutant proteins, *J. Mol. Biol. 307*, 899−911.
12. Benton, C. B., King, J., and Clark, P. L. (2002) Characterization of the protrimer intermediate in the folding pathway of the interdigitated β-helix tailspike protein, *Biochemistry 41*, 5093−5103.
13. Rodriguez-Casado, A., Moore, S. D., Prevelige, P. E., Jr., and Thomas, G. J., Jr. (2001) Structure of bacteriophage P22 portal protein in relation to assembly: Investigation by Raman spectroscopy, *Biochemistry 40*, 13583−13591.
14. Moore, S. D., and Prevelige, P. E., Jr. (2002) Bacteriophage P22 portal vertex formation in vivo, *J. Mol. Biol. 315*, 975−994.
15. Bazinet, C., and King, J. (1985) The DNA translocating vertex of dsDNA bacteriophages, *Annu. Rev. Microbiol. 39*, 109−129.
16. Moore, S. D., and Prevelige, P. E., Jr. (2002) DNA packaging: A new class of molecular motors, *Curr. Biol. 12*, R96−R98.
17. Simpson, A. A., Tao, Y., Leiman, P. G., Badasso, M. O., He, Y., Jardine, P. J., Olson, N. H., Morais, M. C., Grimes, S., Anderson, D. L., Baker, T. S., and Rossmann, M. G. (2000) Structure of the bacteriophage ϕ29 DNA packaging motor, *Nature 408*, 745−750.
18. Morais, M. C., Tao, Y., Olson, N. H., Grimes, S., Jardine, P. J., Anderson, D. L., Baker, T. S., and Rossmann, M. G. (2001) Cryoelectron-microscopy image reconstruction of symmetry mismatches in bacteriophage ϕ29, *J. Struct. Biol. 135*, 38−46.
19. Simpson, A. A., Leiman, P. G., Tao, Y., He, Y., Badasso, M. O., Jardine, P. J., Anderson, D. L., and Rossmann, M. G. (2001) Structure determination of the head−tail connector of bacteriophage ϕ29, *Acta Crystallogr. D 57*, 1260−1269.
20. Guasch, A., Pous, J., Ibarra, B., Gomis-Ruth, F. X., Valpuesta, J. M., Sousa, N., Carrascosa, J. L., and Coll, M. (2002) Detailed architecture of a DNA translocating machine: The high-resolution structure of the bacteriophage ϕ29 connector particle, *J. Mol. Biol. 315*, 663−676.
21. Prevelige, P. E., Jr., Thomas, D., King, J., Towse, S. A., and Thomas, G. J., Jr. (1993) Subunit conformational changes accompanying bacteriophage P22 capsid maturation, *Biochemistry 32*, 537−543.
22. Sambrook, J., Fritsch, E. F., and Maniatis, T. (1989) *Molecular Cloning: A Laboratory Manual*, Cold Spring Harbor Laboratory Press, Cold Spring Harbor, NY.
23. Casjens, S., Wyckoff, E., Hayden, M., Sampson, L., Eppler, K., Randall, S., Moreno, E. T., and Serwer, P. (1992) Bacteriophage P22 portal protein is part of the gauge that regulates packing density of intravirion DNA, *J. Mol. Biol. 224*, 1055−1074.
24. Gill, S. C., and von Hippel, P. H. (1989) Calculation of protein extinction coefficients from amino acid sequence data, *Anal. Biochem. 182*, 319−326.
25. Movileanu, L., Benevides, J. M., and Thomas, G. J., Jr. (1999) Temperature dependence of the Raman spectrum of DNA. I. Raman signatures of premelting and melting transitions of poly(dA-dT)·poly(dA-dT), *J. Raman Spectrosc. 30*, 637−649.
26. Overman, S. A., and Thomas, G. J., Jr. (1999) Raman markers of nonaromatic side chains in an α-helix assembly: Ala, Asp, Glu, Gly, Ile, Leu, Lys, Ser, and Val residues of phage fd subunits, *Biochemistry 38*, 4018−4027.
27. Li, H., and Thomas, G. J., Jr. (1991) Cysteine conformation and sulfhydryl interactions in proteins and viruses. I. Correlation of the Raman S−H band with hydrogen bonding and intramolecular geometry in model compounds, *J. Am. Chem. Soc. 113*, 456−462.
28. Clark, A. J., Inwood, W., Cloutier, T., and Dhillon, T. S. (2001) Nucleotide sequence of coliphage HK620 and the evolution of lambdoid phages, *J. Mol. Biol. 311*, 657−679.
29. Gregoret, L. M., Rader, S. D., Fletterick, R. J., and Cohen, F. E. (1991) Hydrogen bonds involving sulfur atoms in proteins, *Proteins 9*, 99−107.
30. King, J., Botstein, D., Casjens, S., Earnshaw, W., Harrison, S., and Lenk, E. (1976) Structure and assembly of the capsid of bacteriophage P22, *Philos. Trans. R. Soc. London Ser. B 276*, 37−49.

BI020678M